



Article

# Preparation and Corrosion Resistance of Superhydrophobic Composite Coatings on Shot-Peened AA 7075-T6 Aluminum Alloy

Ke Zhan <sup>1,\*</sup>, Ruiqing Ding <sup>1</sup>, Ziliang Liu <sup>1</sup>, Qingchao Yang <sup>1</sup> and Vincent Ji <sup>2,\*</sup>

<sup>1</sup> School of Materials and Chemistry, University of Shanghai for Science and Technology, 516 Jungong Road, Shanghai 200093, China; 223353133@st.usst.edu.cn (R.D.); 233393178@st.usst.edu.cn (Z.L.); 212203100@st.usst.edu.cn (Q.Y.)

<sup>2</sup> ICMMO, UMR CNRS 8182, University Paris Saclay, Bat 410, 91400 Orsay, France

\* Correspondence: zhanke@usst.edu.cn (K.Z.); vincent.ji@u-psud.fr (V.J.)

**Abstract:** In order to further improve the corrosion resistance of 7075-T6 aluminum alloy after shot peening, corrosion-resistant superhydrophobic coatings (EP-HDTMS@SiO<sub>2</sub>) containing epoxy resin (EP), cetyltrimethoxysilane (HDTMS), and nano-silica (SiO<sub>2</sub>) were prepared by a simple spraying method on the surface of shot-peened AA 7075-T6 aluminum alloy. The effects of different EP/SiO<sub>2</sub> mass ratios on the micro-morphology, surface wettability, and corrosion resistance of the superhydrophobic composite coatings were analyzed. Due to the combination of microstructure and the modification of low surface energy organics, the contact angle of EP-HDTMS@SiO<sub>2</sub> coatings reached the superhydrophobic level (152.6°). The electrochemical tests showed that the corrosion current densities ( $I_{\text{corr}}$ ) of the EP-HDTMS@SiO<sub>2</sub> composite coatings were both significantly lower than those of the EP-HDTMS coatings and matrix aluminum alloys. The addition of SiO<sub>2</sub> nanoparticles could improve the hydrophobicity and corrosion resistance of epoxy-based composite coatings. Due to the increase in surface roughness and epoxy resin, the shot-peened AA 7075-T6 alloy coating had high adhesion after the peel test. The prepared coatings also showed excellent corrosion resistance in the neutral salt spray test. This study provides a simple method for preparing stable superhydrophobic coatings on metal surfaces, which is expected to expand the application of 7075 aluminum alloy in harsh environments.

**Keywords:** aluminum alloy; superhydrophobic; silica@epoxy resin; protective coating; salt spray test



**Citation:** Zhan, K.; Ding, R.; Liu, Z.; Yang, Q.; Ji, V. Preparation and Corrosion Resistance of Superhydrophobic Composite Coatings on Shot-Peened AA 7075-T6 Aluminum Alloy. *J. Compos. Sci.* **2024**, *8*, 502. <https://doi.org/10.3390/jcs8120502>

Academic Editor: Jing Shi

Received: 10 October 2024

Revised: 11 November 2024

Accepted: 27 November 2024

Published: 2 December 2024



**Copyright:** © 2024 by the authors. Licensee MDPI, Basel, Switzerland. This article is an open access article distributed under the terms and conditions of the Creative Commons Attribution (CC BY) license (<https://creativecommons.org/licenses/by/4.0/>).

## 1. Introduction

7075 aluminum alloy is a Al-Zn-Mg-Cu ultra-high strength aluminum alloy, which is widely used in the aircraft industry [1]. 7075 aluminum alloy also has good corrosion resistance, but has a certain tendency for stress corrosion. In particular, Cl<sup>-</sup> often leads to local pitting corrosion, intergranular corrosion (IGC), or stress corrosion cracking (SCC), which significantly affects the safety performance and service life of the components in marine environments [2–4]. Corrosion pits usually initially form at surface defects and often act as stress concentration locations, where cracks are more likely to form under external loads or tensile residual stresses. Theoretically, the stress corrosion behavior of aluminum alloy depends not only on the composition of the grain boundaries, the grain structure, and precipitated phase, but also on surface conditions such as residual stress and surface roughness [5–7]. Therefore, AA 7075-T6 aluminum alloy is expected to improve corrosion resistance through appropriate subsequent surface treatment.

Previous research has investigated the influence of various parameters of shot peening on stress corrosion behavior. Bao et al. [8] showed that the compressive residual stress and surface roughness of aluminum alloy AA 7075-T6 were influenced by the diameter of shots and the intensity of shot peening. Compared with the single shot-peening process,

the dual shot-peening process had a higher compressive residual stress value and a lower surface roughness. In terms of the number and depth of cracks, it showed relatively better resistance to stress corrosion; however, all shot-peened samples showed surface pitting corrosion. The increased surface roughness often accelerated the process of localized pitting corrosion [9–11]. Sajid et al. [12] found that after improving the surface roughness of ASTM A36 steel, the local corrosion pitting tendency was alleviated. It was shown that the increased surface roughness could improve the wettability of the steel and thereby promote the corrosion process. In contrast, samples with lower surface roughness are significantly less susceptible to pitting corrosion, indicating that surface roughness is one of the important factors affecting the degree of surface corrosion pitting. Walter et al. [13] investigated the effect of surface roughness on the passivation and pitting behavior of AZ91 magnesium alloy in a chlorine-containing environment. As the surface roughness of magnesium alloy increased, the pitting tendency of the alloy also increased.

Due to their special surface wettability, superhydrophobic coatings have a lot of potential for applications in different fields, such as anti-corrosion [14], self-cleaning [15], anti-pollution [16], anti-icing [17], and drag reduction [18]. Inspired by the natural material template of lotus, researchers constructed an artificial superhydrophobic coating with a contact angle ( $>150^\circ$ ) and a low sliding angle ( $<10^\circ$ ) through a combination of a low-surface energy materials and a micro-nano bilayer coarse structure. In recent years, the application of superhydrophobic coatings in the corrosion protection of metal alloys has attracted great attention. The superhydrophobic coating can make the corrosion liquid to form a ball on the surface and slide off easily, thereby reducing the contact area and contact time between the corrosive medium and the protected surface [19]. In acidic water and seawater, the superhydrophobic film layer has a good barrier effect against chloride ions and acid-alkaline corrosive media, which can effectively inhibit the corrosion process and is expected to change the surface wettability and significantly improve the corrosion resistance of metal alloy [20].

Many methods for producing superhydrophobic coatings have been proposed so far. Compared with other methods, the spraying method is simple, low cost, and highly compatible with various substrates. The spraying method is considered as an important process for the large-scale production of superhydrophobic coatings on aluminum alloys [21]. However, the solvents and additives with low surface energy used in the preparation process are more expensive and usually contain fluorine or silane compounds, which cause varying degrees of environmental impact. As a low surface energy additive, hexadecyltrimethoxysilane is inexpensive, environmentally friendly, and is widely used as a superhydrophobic modification agent [22–24]. There are many nanoadditives available to modify the wettability of coatings, such as graphene and carbona [25,26], but they are expensive to prepare and have problems with dispersion and stability in some cases.  $\text{SiO}_2$  nanoparticles have excellent chemical stability, good dispersion in organic solvents and polymer matrices, are more likely to form homogeneous micro-nanostructures in coatings, and are relatively inexpensive and environmentally friendly, making  $\text{SiO}_2$  nanoparticles a very attractive option. Shells are composed of nanoparticles and polymers [27], and HDTMS@ $\text{SiO}_2$  coatings have a particle/polymer design similar to the microstructure of simulated shells, and thus they exhibit excellent corrosion resistance and superhydrophobicity like shells.

In this research, a single-step spraying technique was used to prepare the superhydrophobic composite coating EP-HDTMS@ $\text{SiO}_2$ , aiming to protect the aluminum alloy 7075-T6 from pitting after shot-peening treatment. The coating suspension contained a fluorine-free modifier, epoxy resin, polyamide, and silica nanoparticles. The wettability, surface morphology, and surface chemical groups of the superhydrophobic coating were characterized, and its corrosion resistance and self-cleaning ability were investigated. Finally, the protection mechanism of the composite coating on the shot-peened aluminum alloy was further analyzed.

## 2. Materials and Methods

### 2.1. Materials

Aluminum alloy AA 7075-T6 was used; the specific composition and content are shown in Table 1. SiO<sub>2</sub> with a diameter of 30 nm, hexadecyltrimethoxysilane (HDTMS), epoxy resin E-44 (C<sub>21</sub>H<sub>24</sub>O<sub>4</sub>), and polyamide 651 ((C<sub>6</sub>H<sub>11</sub>NO)<sub>n</sub>) were purchased from Shanghai Yi En Chemical Technology Co., Ltd., Shanghai, China. Ammonia, sodium chloride (NaCl), and anhydrous ethanol were supplied by Sinopharm Group Chemical Reagent Co., Ltd., Ningbo, China. All reagents were used as received and no further purification was required.

**Table 1.** Composition and mass fractions of AA 7075-T6 aluminum alloy.

Element	Cu	Mn	Mg	Zn	Cr	Ti	Si	Fe
Content	1.2–2.0	0.30	2.1–2.9	5.1–6.1	0.18–0.28	0.20	0.40	0.50

### 2.2. Pre-Treatment of AA 7075-T6 Samples

AA 7075-T6 aluminum alloy samples were cut into blocks of 15 mm × 15 mm × 3 mm and polished with silicon carbide (SiC) abrasive paper (320, 800, and 2000 mesh numbers in sequence). Ultrasonic washing with acetone and ethanol for 15 min was applied to remove oil and stains. The surface of AA 7075-T6 aluminum alloy was treated with an air blasting machine from Kunshan Kasi Machinery Co., Ltd. in Suzhou, Jiangsu, China. The 0.18 mm ceramic balls were used, and the distance between the nozzle and the sample was 100 mm. The air pressure was 0.40 MPa, and the surface coverage of the shot-peening process was 100%. The prepared shot-peening sample was cleaned with ultrasonic waves in anhydrous ethanol for 10 min and then dried in cold air.

### 2.3. Preparation of EP-HDTMS@SiO<sub>2</sub> Superhydrophobic Coatings

SiO<sub>2</sub> nanoparticles with a weight of 0.6 g were ultrasonically dispersed in 25 mL of anhydrous ethanol for 30 min, and then HDTMS (0.8 g) was added into the solution. To promote the hydrolysis of HDTMS, the solution pH was adjusted to 7.6 by adding 1 mL of NH<sub>3</sub>-H<sub>2</sub>O at a concentration of 4 mol/L. The reaction lasted 12 h under constant magnetic stirring at room temperature, and an HDTMS-modified hydrophobic SiO<sub>2</sub> particle suspension was obtained. At the same time, epoxy resin (0.9 g) was added and mixed for 6 h with magnetic stirring. Before spraying treatment, the curing agent (0.45 g) was added to the mixing solution and mixed by ultrasonication at room temperature for 20 min to form an emulsion (i.e., paint). The emulsion was introduced into the barrel of the spray gun and, with a nozzle diameter of 1 mm and a pressure of 0.2 MPa, the suspended solution was sprayed about 10 cm away from the aluminum alloy plate. Numerous experiments and studies have shown that 60 °C and 12 h are the optimal curing conditions, so the coating samples were placed in a 60 °C oven and held for 12 h.

The formation mechanism of the superhydrophobic EP-HDTMS@SiO<sub>2</sub> coating can be explained as follows: under the catalysis of an alkaline solution, a long chain of HDTMS silane was hydrolyzed to a cetylsilanol. Each cetylsilanol contained three -OH groups and the silanol molecules reacted with each other to form polysiloxanes. On the other hand, due to the hydrophilicity of SiO<sub>2</sub>, SiO<sub>2</sub> particles adsorbed a large amount of (-OH), which can be bonded with hydrogen on the surface of the solution. Finally, the long-chain silane condensed with SiO<sub>2</sub> particles to form Si-O-Si three-dimensional network structure nanoparticles [23]. Under the joint action of hydrophobic groups and hydroxyl groups, small gaps emerged between silica particles. These small gaps were filled with air and formed a micro-rough structure on the surface, achieving superhydrophobicity. The processing is shown in Figure 1.

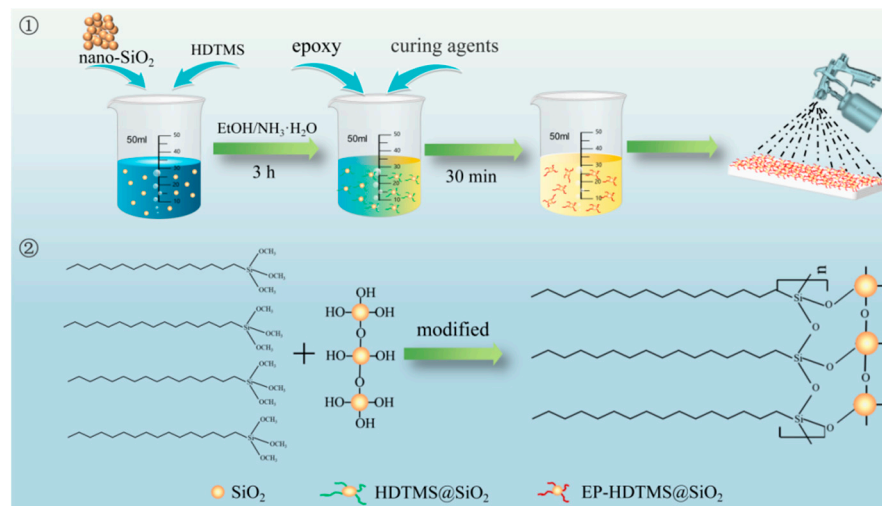


**Figure 1.** Processing to prepare superhydrophobic EP-HDTMS@SiO<sub>2</sub> coatings on shot-peened 7075-T6 aluminum alloy. (1. Mechanism of Superhydrophobic EP-HDTMS@SiO<sub>2</sub> Coating Formation. 2. Processing of Superhydrophobic EP-HDTMS@SiO<sub>2</sub> Coating.).

#### 2.4. Characterization

The surface morphology of the superhydrophobic EP-HDTMS@SiO<sub>2</sub> coating before and after the corrosion test was characterized using a field emission scanning electron microscope (Thermo Fisher Scientific, Nova Nano-450, Waltham, MA, USA) and an energy dispersive spectrometer (EDS, FEI, Nova Nano-450, USA). The water contact angle (WCA) of the prepared sample was measured using a 1  $\mu$ L water drop with an interfacial tension meter (JC2000C1). A Fourier transform infrared spectrometer (FT-IR, Perkin Elmer Waltham, MA, USA) was used to analyze the chemical structure by characterizing the power scraped from the surface. The chemical composition of the composite coating was determined by X-Ray photoelectron spectroscopy (XPS, Thermo Scientific, K-Alpha, Waltham, MA, USA). The corrosion products of the aluminum alloy after the salt spray test were determined using an X-Ray diffractometer (XRD, D8 Advance Bruker AXS, Karlsruhe, Germany).

The electrochemical behavior of prepared samples was examined in a 3.5 wt% NaCl solution using an electrochemical workstation (CHI600e). The edge of the sprayed sample was sealed with wax oil to ensure that the exposed area was 1 cm<sup>2</sup>. The operational setup consists of a standard measurement configuration with three electrodes, a counter electrode made of platinum, a reference electrode in the form of a saturated calomel electrode, and a working electrode that represents the sample itself. Polarization measurements were performed at a constant voltage sweep rate of 0.5 mV/s, allowing the calculation of the corrosion current density ( $I_{\text{corr}}$ ) through the cathode-tan slope. In addition, electrochemical impedance spectroscopy (EIS) was performed in a frequency range of 10<sup>-2</sup> to 10<sup>5</sup> Hz using a polarization curve potential design of -1.6 to 0.2 V and an AC amplitude of 20 mV. To ensure the stability of the coating data, the sample was placed in an NaCl solution for 10 min before each electrochemical test. Zview software (2.0.0.10) was used to analyze and adjust the impedance spectrum of the sample. A KE-60B salt spray test machine (Foshan Huahe Vibration Testing Machine Manufacturing Co., Ltd., Foshan, Guangdong, China) was used for the salt spray test.

### 3. Results and Discussion

#### 3.1. Surface Morphology of EP-HDTMS@SiO<sub>2</sub> Coatings

As shown in Figure 2(a<sub>1</sub>,a<sub>2</sub>), without the addition of SiO<sub>2</sub>, the surface of the aluminum alloy was covered with an organic coating mainly composed of epoxy resin that was evenly distributed and flat, and had a good overall appearance. However, upon careful observation, it can be seen that there were some small pores in the coating, which were probably due to the pores formed by the evaporation process of anhydrous ethanol. The

addition of nano-silicon dioxide made the surface contour of the coating rough, and valleys and micro peaks (several hundred nano-meters high) can be clearly seen with the SEM. When the mass ratio of EP to SiO<sub>2</sub> reaches 1.5, as shown in Figure 2(b<sub>1</sub>), the accumulated nanoparticles of SiO<sub>2</sub> modified by HDTMS form many irregular structures, providing a rough structure and enough air pockets on the surface to achieve hydrophobicity. However, after superhydrophobic modification, some nanoparticles agglomerated to a certain extent and formed micro-sized agglomerates. These clusters were mainly composed of modified HDTMS@SiO<sub>2</sub> coated with epoxy resin (shown in Figure 2(b<sub>2</sub>)). The contact angle measured here was below 120° because the epoxy content significantly exceeded the silica content. This suggested that obtaining a superhydrophobic rough surface structure is essential for low surfaces. Comparing Figure 2(c<sub>2</sub>,d<sub>2</sub>,e<sub>2</sub>), it can be found that the surface roughness of the composite coating was higher compared to Figure 2(b<sub>2</sub>), which allowed air transport and resulted in a larger contact angle on the surface of the composite coating. When a water droplet was introduced into the EP-HDTMS@SiO<sub>2</sub> coating, only a small part of it came into contact with the protruding micro/nano-structures, thereby reducing the contact area between the droplet and the nano-composite coating. As a result, the EP-HDTMS@SiO<sub>2</sub> nano-composite coating exhibited excellent superhydrophobicity with a contact angle of up to 150°. However, looking at Figure 2(c<sub>1</sub>), one can see that there were some subtle cracks in the coating at this point. These cracks divided the entire surface coating into fragments due to the further increase in nanoparticles, making their distribution difficult. At the same time, the lack of epoxy resin in the composite coating can also cause cracks in the coating surface. These cracks in the film can be caused by volume shrinkage due to the evaporation of ethanol in the film. Therefore, excessive addition of silica and relative reduction in epoxy resin did not have a positive effect on the integrity of the coating.

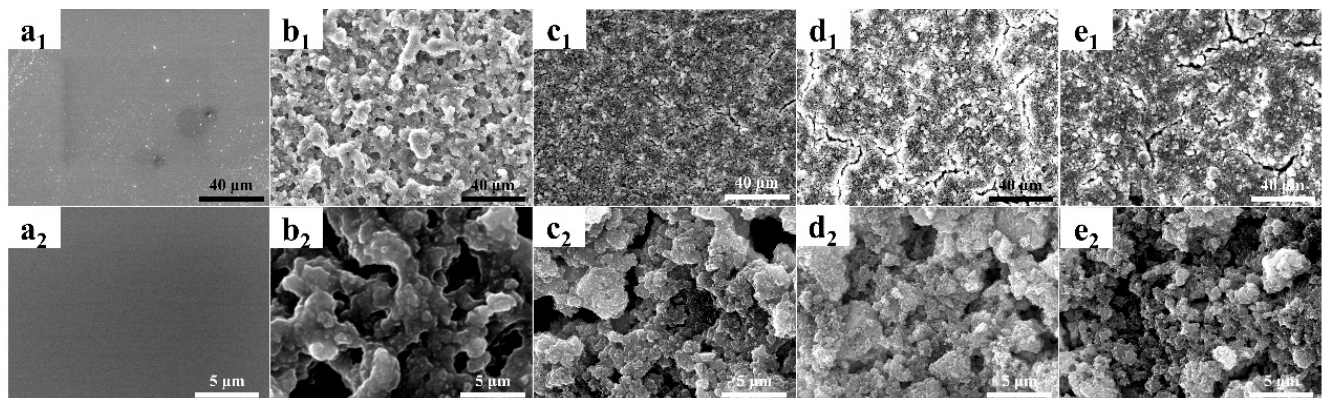


**Figure 2.** Low and high magnification SEM images of EP/SiO<sub>2</sub> composite coatings with different ratios, (a<sub>1</sub>,a<sub>2</sub>) no SiO<sub>2</sub> was added; (b<sub>1</sub>,b<sub>2</sub>) 3:1; (c<sub>1</sub>,c<sub>2</sub>) 3:2; (d<sub>1</sub>,d<sub>2</sub>) 1:1; (e<sub>1</sub>,e<sub>2</sub>) 3:4.

### 3.2. Chemical Composition of EP-HDTMS@SiO<sub>2</sub> Coatings

As shown in the figure, only the elements C, O, and Si were detected in the spectra without the addition of nano-SiO<sub>2</sub> with atomic percentages of 84.84%, 13.95%, and 1.21%, respectively. However, it is clear from the EP-HDTMS@SiO<sub>2</sub> in Figure 3b that the proportions of the three main elements C, O, and Si are 59.08%, 29.95%, and 10.69%, respectively. The initially small amount of silicon element contained is mainly due to the small amount of Si element contained in hexadecyltrimethoxysilane. The significant increase in the content of O and Si elements in Figure 3b is due to the addition of SiO<sub>2</sub>. From the distribution of nanoparticle elements in Figure 3c, it can be seen that the C, O, and Si indicate relatively uniform distribution of the coating by spraying.

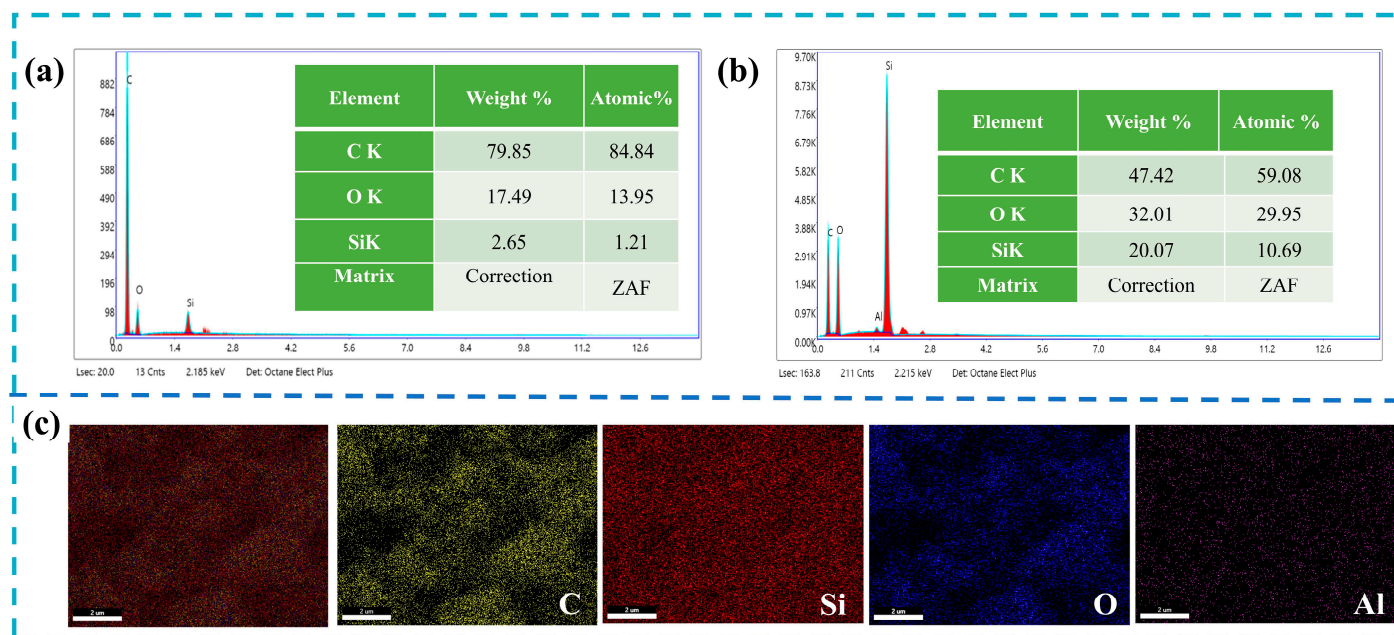


**Figure 3.** (a,b) EDS without nanosized SiO<sub>2</sub> and EP/SiO<sub>2</sub> mass ratio of 3:2; (c) mapping with an EP/SiO<sub>2</sub> ratio of 3:2.

The FT-IR test results are shown in Figure 4. The characteristic peaks of SiO<sub>2</sub> include a stretching vibration peak of 3440 cm<sup>-1</sup> for -OH, a bending vibration peak of 1627 cm<sup>-1</sup> for H-OH, an asymmetric stretching vibration peak of 1100 for Si-O-Si, a stretching vibration peak of Si-O-Si bonds at 802 cm<sup>-1</sup>, and a bending vibration peak of Si-O-Si bonds at 470 cm<sup>-1</sup>. At 1464 cm<sup>-1</sup>, a new band formed due to the stretching vibration of the C-O group, indicating a covalent bond between the Si-OH group and the hexadecyl group of HDTMS [28]. More importantly, two new bands were discovered at 2922 and 2852 cm<sup>-1</sup>, attributed to the stretching vibrations in the -CH<sub>3</sub> and -CH<sub>2</sub> bands of HDTMS, respectively. Especially, according to the FT-IR spectrum of SiO<sub>2</sub>, the absorption peak at 1700 cm<sup>-1</sup> was carbonyl (C=O stretching), indicating that the double bonds in the carbonyl group were unstable [29]. For superhydrophobic EP-HDTMS@SiO<sub>2</sub> coatings, the characteristic absorption peak intensity of the Si-O bonds gradually increased, indicating that the nano-SiO<sub>2</sub> particles were successfully grafted onto the surface.

The chemical composition of the superhydrophobic EP-HDTMS@SiO<sub>2</sub> coating was further determined and characterized using XPS in Figure 5. The C1s energy level spectrum of the superhydrophobic EP-HDTMS@SiO<sub>2</sub> coating can be curve-fitted into three peak components, and the BEs of the C-Si, C-C, and C-O double bonds were 283.0 eV, 284.5 eV, and 286.4 eV, respectively [30]. The Si-2p spectra showed peak components at BEs of 103, 103.5, and 102.7 eV, corresponding to Si-O, Si-O-Si, and Si-O-C, respectively. Furthermore, the superhydrophobic coating EP-HDTMS@SiO<sub>2</sub> exhibited both Si-O-Si and Si-O-C peak components, indicating the presence of low surface energy silanes on the composite coatings [31]. The above results showed that HDTMS had successfully completed the modification through the covalent interaction between the silanol groups of the silane agent and SiO<sub>2</sub> [10], which were consistent with the previous FT-IR characterization.

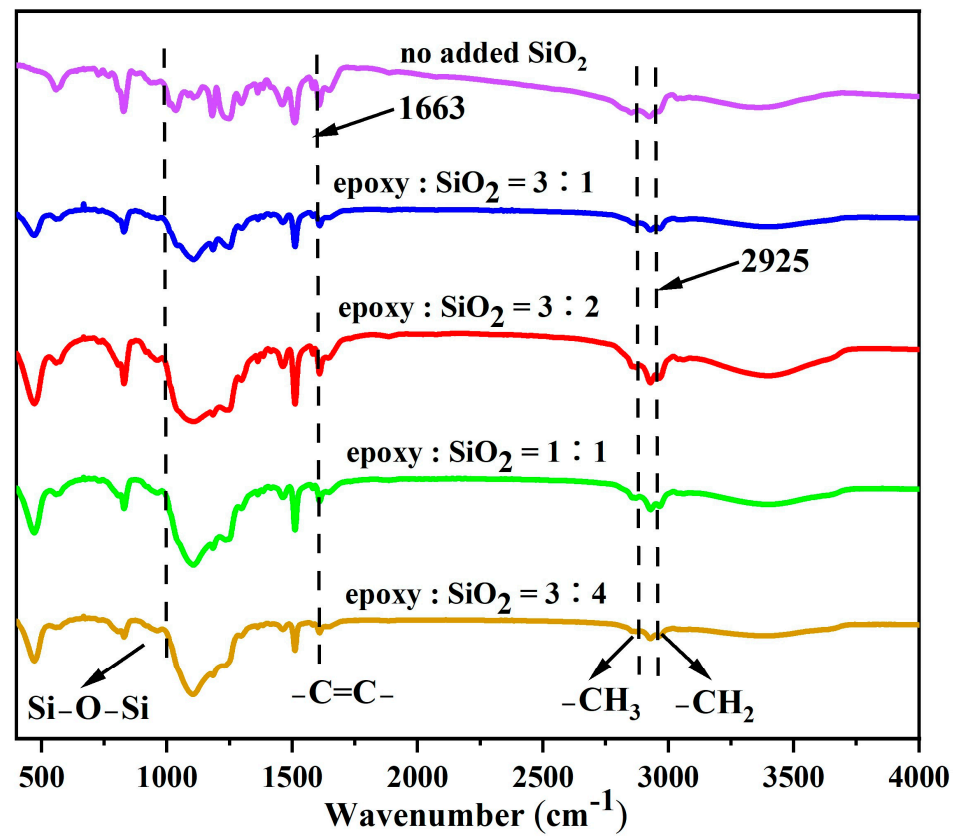


Figure 4. EP-HDTMS@SiO<sub>2</sub> FT-IR spectroscopy of superhydrophobic coatings.

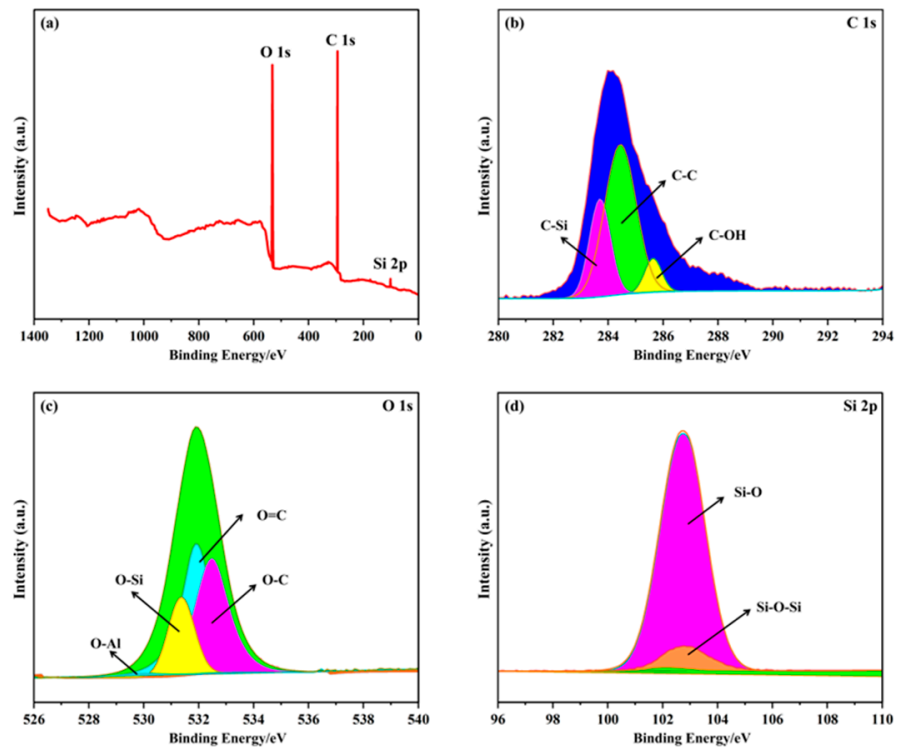
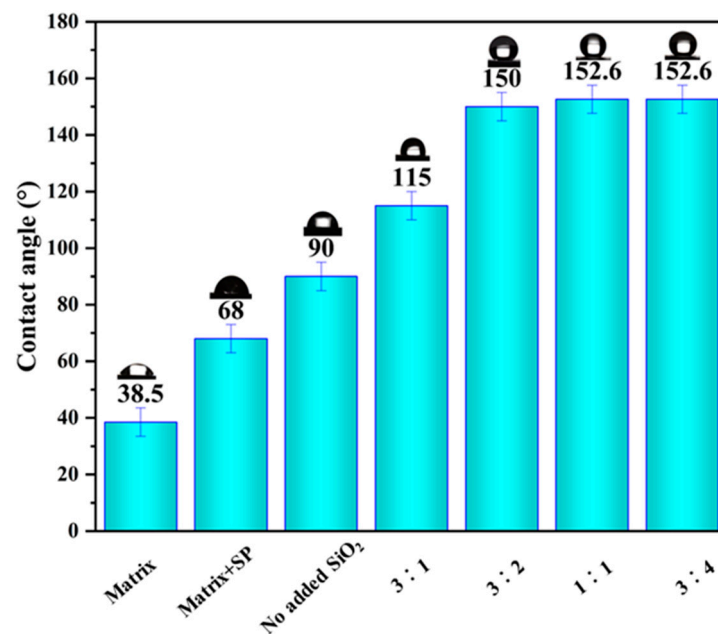


Figure 5. EP-HDTMS@SiO<sub>2</sub> XPS of superhydrophobic coatings: (a) full spectrum; (b) C 1s; (c) O 1s; (d) Si 2p.

### 3.3. Wettability of EP-HDTMS@SiO<sub>2</sub> Coatings

To investigate the influence of the mass ratio of EP and SiO<sub>2</sub> on the EP-HDTMS@SiO<sub>2</sub> coatings, samples with different mass ratios were prepared. The mass ratios of unadded SiO<sub>2</sub> and EP/SiO<sub>2</sub> were adjusted to 3:1, 3:2, 1:1, and 3:4 for a total of five groups, with the other components remaining unchanged. The results of the contact angle test are shown in Figure 6. The aluminum alloy surface showed good wettability with a contact angle of only 38.5° due to its low surface energy and high flatness. Pretreatment by shot peening increased the surface roughness and specific surface area, thereby increasing the surface energy. After shot-peening treatment, the contact angle increased to 68° and still showed hydrophilicity, indicating that the shot-peening method can change the wettability of the surface. Without the addition of nanoparticles, the contact angle of the epoxy resin coating was 90°, indicating that the epoxy resin itself had some hydrophilicity. By adding SiO<sub>2</sub> nanoparticles, the contact angle on the surface of the epoxy resin composite coatings could be significantly improved. As the amount of SiO<sub>2</sub> particles increased, the contact angle on the surface of the epoxy resin composite coating gradually increased. At a mass ratio of 3:2, the surface hydrophobicity of the nano-composite coating reached up to 150°, achieving superhydrophobicity. When the mass ratio of EP/SiO<sub>2</sub> nanoparticles was 1:1, the surface hydrophobicity of the nano-composite coating was the best with a WAC of 152°. This was because as the mass of EP-SiO<sub>2</sub> nanoparticles increased, not only did the surface roughness of the nano-composite coating improve, but also the content of HDTMS grafted on SiO<sub>2</sub> nanoparticles increased, which further reduced the surface energy. Consequently, the EP-HDTMS@SiO<sub>2</sub> nano-composite coating exhibited superhydrophobicity.



**Figure 6.** WAC data of aluminum alloy, pretreated aluminum alloy, and coated surface with different contents of SiO<sub>2</sub> nanoparticles.

As the mass ratio of EP to SiO<sub>2</sub> continued to increase, the water contact angle (WAC) of the nano-composite EP-HDTMS@SiO<sub>2</sub> coating did not increase further and remained at about 152.6°. This phenomenon may be due to the fact that when the mass of SiO<sub>2</sub> nanoparticles increased to a certain level, the excessive number of nanoparticles prevented them from effectively adhering to the EP-HDTMS@SiO<sub>2</sub> coating. A further increase in nanoparticle mass may complicate the dispersion of nanoparticles, which may be due to increased interactions between nanoparticles, making it difficult for them to disperse evenly throughout the coating. This experiment could meet the requirements of superhydrophobicity under certain addition ratios.

### 3.4. Wettability of EP-HDTMS@SiO<sub>2</sub> Coatings with Different Solutions

To study the influence of pH on the contact angle of droplets of a superhydrophobic surface solution, acidic solutions with pH 1 ~ 6 were prepared with HCl solution, solutions with pH 8~14 were prepared with NaOH solution, and the liquid with pH 7 was ultrapure water. Through experiments, we found that the EP-HDTMS@SiO<sub>2</sub> coating showed good superhydrophobic properties in solutions with different pH values. In particular, when the pH value of the solution was in the range of 1 to 13, the contact angle of the droplets on the coating surface was larger than 140°, indicating that the coating has excellent resistance to both acidic and alkaline solutions, as shown in Figure 7a. Furthermore, common household liquids such as tea, coffee, milk, Coca-Cola, and salt water all showed extremely low adhesion to the surface of the prepared superhydrophobic coating, as shown in Figure 7b. These droplets could exist in a spherical shape on the surface of the coating and show the unique properties of an ultra-wet-phobic surface. Compared to other liquids, milk resulted in a smaller contact angle on the coated surface, indicating that milk had better diffusion and wettability on the coated surface. This phenomenon may be related to the molecular structure and composition of milk, such as sugar molecules, fats, etc.

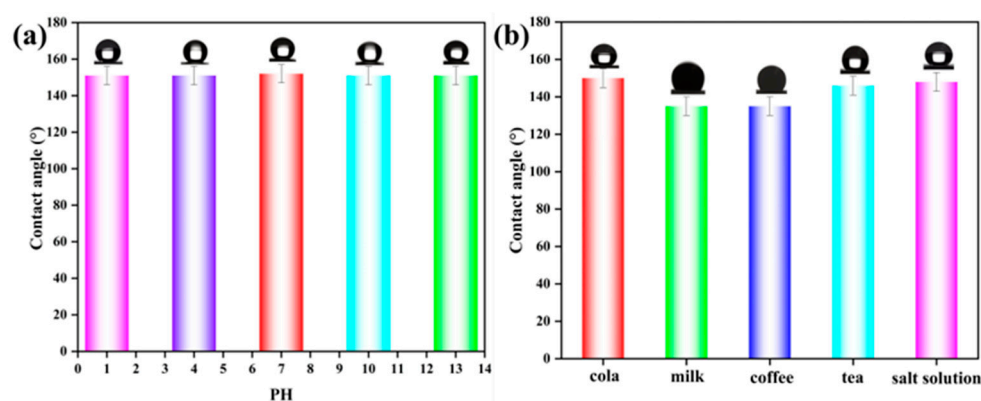


**Figure 7.** Wettability of EP-HDTMS@SiO<sub>2</sub> superhydrophobic coating with 3:2 mass ratio of EP to SiO<sub>2</sub> on different liquids: (a) different pH; (b) different solutions.

### 3.5. Electrochemical Behavior of EP-HDTMS@SiO<sub>2</sub> Coatings

The electrochemical behavior of different mass ratios of EP to SiO<sub>2</sub> was investigated using electrochemical impedance spectroscopy. The Nyquist plot and Bode plot of the measured EIS data are shown in Figure 8. For the Nyquist diagram, the larger the impedance arc radius, the higher the corrosion resistance. At an EP to SiO<sub>2</sub> mass ratio of 1.5, the EP-HDTMS@SiO<sub>2</sub> coating exhibited the highest antipolarization performance. It can be seen from Figure 8a that the Nyquist curve was semicircular when the mass ratio of EP to SiO<sub>2</sub> was a maximum, and the diameter of the semicircular curve can usually be regarded as the resistance value of the test materials. The Nyquist curve of other coatings with different proportions consists of a semicircle and a tail, which is the “semicircle + tail” curve. According to the fitting circuit analysis, the corrosion resistance of the coating was mainly related to the internal resistance  $R_1$  of the coating. The resistance values  $R_1$  are listed in Table 2. The  $R_1$  of all coatings with added SiO<sub>2</sub> nanoparticles was higher than that of EP-HDTMS coatings, indicating that the addition of SiO<sub>2</sub> can improve the corrosion resistance of the coatings. As the content of SiO<sub>2</sub> nanoparticles increased, the internal resistance  $R_1$  first increased and then decreased, reaching its maximum value of 52 W  $\Omega$  at 3:1. The rapid drop in internal resistance  $R_1$  was related to the cracking caused by the insufficient amount of epoxy resin. The NaCl solution appears to quickly diffuse into the epoxy resin layer and reach the substrate. Figure 8b shows the phase angle curves of composite coatings prepared with different ratios. At high frequencies, the phase angle of the EP-HDTMS@SiO<sub>2</sub> coating approaches 90°, indicating that the coating acted as a perfect capacitor. At a mass ratio of EP to SiO<sub>2</sub> of 1.5, the phase angle of the coating remained at a high level over a wide

intermediate frequency range. In the Bode diagram, the impedance modulus  $|Z|$  at low frequencies can typically represent the corrosion resistance of superhydrophobic coatings. From the graph, it can be seen that the EP-HDTMS@SiO<sub>2</sub> coating achieved the highest resistance when the mass ratio of EP to SiO<sub>2</sub> was 1.5. For the quantitative analysis, the  $Z_{view}$  equivalent circuit was used to accurately fit the EIS, as shown in Figure 8d. Among them, the  $R_s$ ,  $R_1$ , and  $R_2$  scans represented the solution resistance, coating resistance, and charge transfer resistance, respectively, while the  $CPE_1$  and  $CPE_2$  types correspond to the coating capacitance and double layer capacitance, respectively.

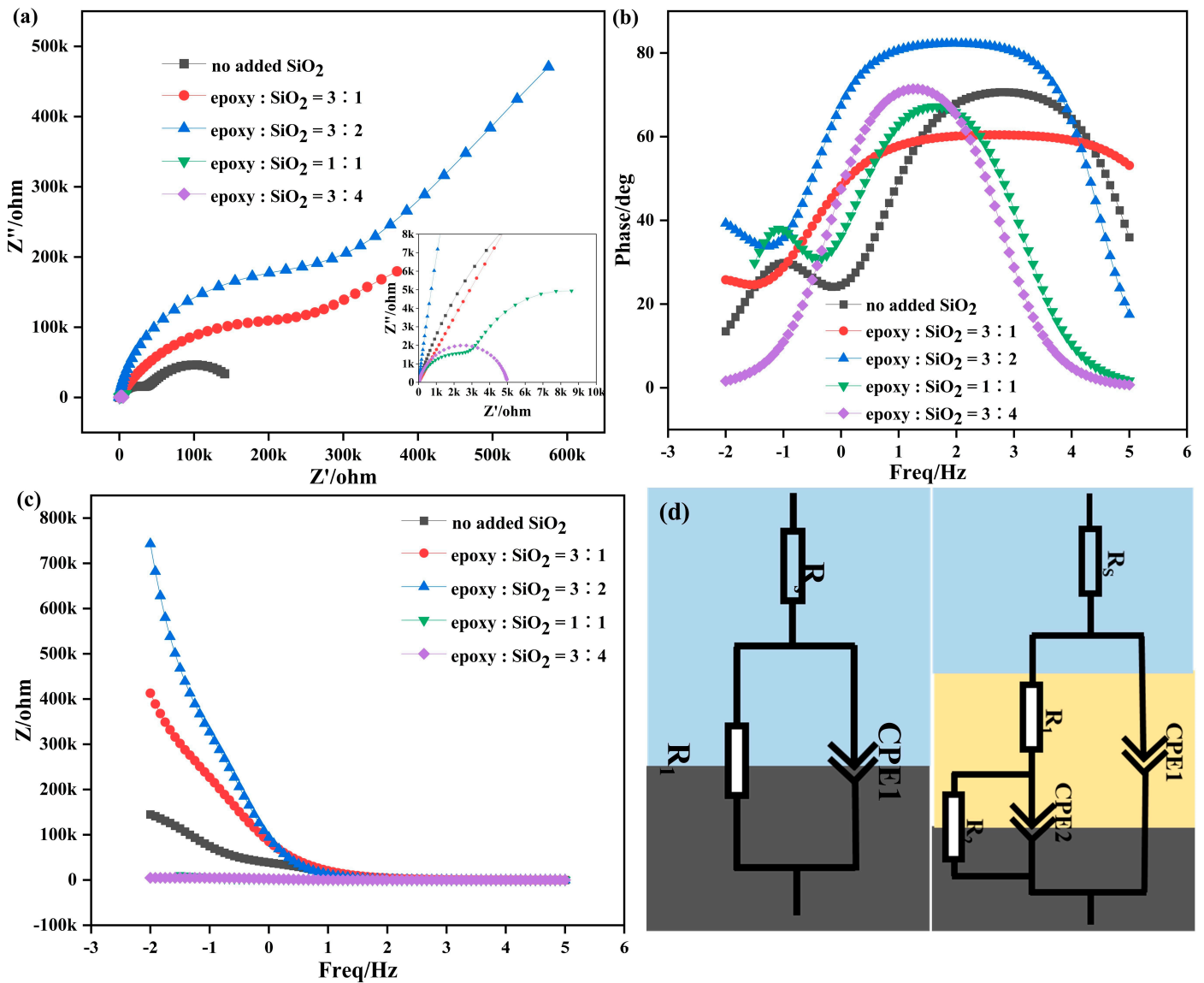


**Figure 8.** (a) Bode impedance plots with different EP/SiO<sub>2</sub> ratios; (b) phase diagram; (c) freq Z diagram; (d) circuit fitting diagram.

**Table 2.** EIS fitting results of coatings with different compositions.

EP:SiO <sub>2</sub>	Without SiO <sub>2</sub>	3:1	3:2	1:1	3:4
$R_s/\Omega$	13.34	7.004	8.492	12.89	13.38
$R_1/\Omega$	41,238	333,640	520,971	3917	5498
$R_2/\Omega$	125,140	583,180	690,701	9919	—

Figure 9 shows the polarization curves of all samples, and the corresponding corrosion potential ( $E_{\text{corr}}$ ) and corrosion current density ( $I_{\text{corr}}$ ) results are shown in Table 3. The corrosion resistance of superhydrophobic EP-HDTMS@SiO<sub>2</sub> coatings was evaluated not only via electrochemical impedance spectroscopy (EIS), but also using dynamic potential polarization (Tafel). In this study, measurements were performed at room temperature in a 3.5% NaCl solution. Figure 8 shows the polarization curves of a superhydrophobic surface with different mass ratios of EP and SiO<sub>2</sub>. Tafel linear extrapolation was used to obtain electrochemical parameters of the samples, mainly including corrosion potential ( $E_{\text{corr}}$ ) and corrosion current density ( $I_{\text{corr}}$ ). The specific values are listed in Table 3. For the Tafel test, an increase in corrosion potential and a decrease in corrosion current represented an improvement in the corrosion resistance of the material. It was not difficult to see that the aluminum alloy after spraying organic coatings, regardless of the mass ratio of EP to SiO<sub>2</sub>, had a more positive  $E_{\text{corr}}$  and a smaller  $I_{\text{corr}}$  compared to pure Al. Without the addition of nano-silica, the  $E_{\text{corr}}$  of the EP-HDTMS coating was  $-0.972$  V and the  $I_{\text{corr}}$  was  $1.321 \times 10^{-7}$  A/cm<sup>2</sup>. When the mass ratio of EP to SiO<sub>2</sub> is 3:1, the minimum  $I_{\text{corr}}$  obtained is  $2.295 \times 10^{-8}$  A/cm<sup>2</sup>. Due to the presence of fine cracks on the surface of the coating, the  $I_{\text{corr}}$  at a mass ratio of EP to SiO<sub>2</sub> of 3:2 was  $2.562 \times 10^{-7}$  A/cm<sup>2</sup>. A surface containing an appropriate amount of nano-silica can effectively improve the corrosion resistance of the coating. Excess silica increased agglomeration and cracking of the coating, resulting in a reduction in the coating's protection of the substrate's corrosion resistance.

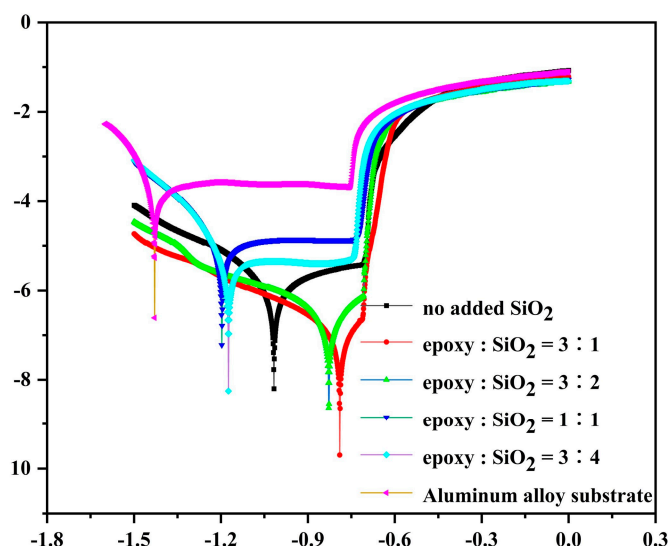


Figure 9. Tafel curves for the coatings and substrate.

Table 3. Tafel corrosion current densities and corrosion potentials for the coatings and substrate.

EP:SiO <sub>2</sub>	Without SiO <sub>2</sub>	3:1	3:2	1:1	3:4	Pure Al
$E_{\text{corr}}$ vs. SCE (V)	$-0.972$	$-0.790$	$-0.828$	$-1.197$	$-1.174$	$-1.429$
$I_{\text{corr}}$ (A cm <sup>-2</sup> )	$1.321 \times 10^{-7}$	$2.295 \times 10^{-8}$	$2.562 \times 10^{-7}$	$8.606 \times 10^{-6}$	$4.097 \times 10^{-6}$	$2.398 \times 10^{-4}$

### 3.6. Self-Cleaning Performance of EP-HDTMS@SiO<sub>2</sub> Coatings

Figure 10 shows the self-cleaning effect of the hydrophobic coating on the surface of the aluminum alloy. When water droplets are applied to an untreated aluminum alloy surface, they diffuse and adhere to the surface, indicating the hydrophilicity of the surface. However, for aluminum alloys coated with the superhydrophobic EP-HDTMS@SiO<sub>2</sub> coating, the water droplets remained spherical and were cut off from the surface with the CuSO<sub>4</sub> powder, revealing its superhydrophobic properties. Under similar conditions, when a drop of water touches a surface made of superhydrophobic aluminum alloy that contains

dirt particles such as toner, soot, and chalk dust, the water drop immediately beads up, taking the attached dirt particles with it. This process left almost no traces of contaminants on the surface, indicating that the adhesion between the contaminant particles and the superhydrophobic surface was weak. It was concluded that the superhydrophobic aluminum alloy coated with EP-HDTMS@SiO<sub>2</sub> had excellent self-cleaning properties. The mechanism for this self-cleaning performance lay in the interaction between the superhydrophobic surface and the rolling water droplets. Since the surface was superhydrophobic, water droplets did not spread upon contact with the surface but remained spherical. At the same time, due to the effect of surface tension, the water droplets reduced their surface area so that they wrapped tightly around the dirt particles and carried them away from the surface. This process not only removed the surface contamination but also ensured that the surface was clean and effectively prevented further contamination.

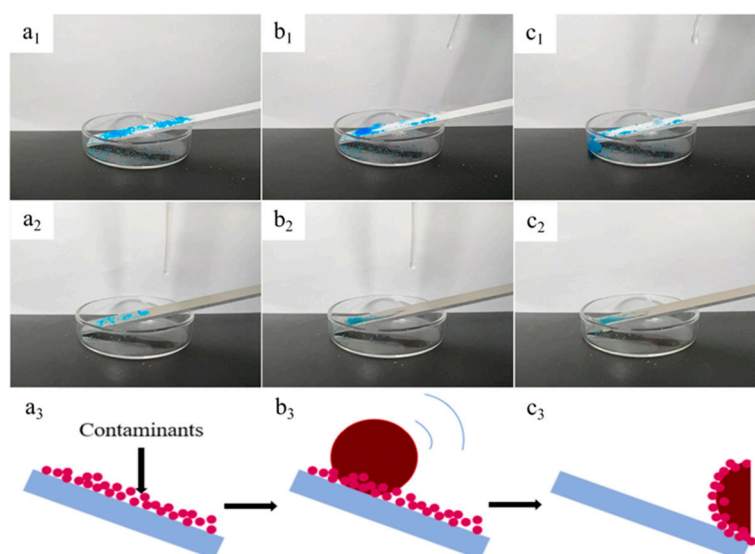


**Figure 10.** (a<sub>1</sub>,b<sub>1</sub>,c<sub>1</sub>) EP-HDTMS@SiO<sub>2</sub> self-cleaning comparison between superhydrophobic coating with 3:2 mass ratio of EP to SiO<sub>2</sub> and substrate (a<sub>2</sub>,b<sub>2</sub>,c<sub>2</sub>), blue powder is CuSO<sub>4</sub>. (a<sub>3</sub>,b<sub>3</sub>,c<sub>3</sub>) Self-cleaning theory diagram.

### 3.7. Adhesion of EP-HDTMS@SiO<sub>2</sub> Coatings

In practical applications, it is crucial to maintain the superhydrophobicity of the surface of superhydrophobic wood under external loads. To investigate mechanical durability, mechanical tests were performed including tape peeling and knife scraping. Tape test: The adhesive strength of the coating was evaluated according to ISO 2409–2007. As shown in the images of Figure 11(a<sub>1</sub>,a<sub>2</sub>), the tape peeling test was carried out by quickly peeling off the surface of superhydrophobic wood by repeatedly applying a high-viscosity tape with fingers. After mixing with epoxy resin, the polyamide hardener chemically reacts to form a high molecular weight polymer. Next came the cross-linking reaction. The polymer materials produced through polymerization reactions ultimately undergo curing reactions. After the cross-linking reaction is complete, the polyamide hardener continues to participate in the curing reaction, making the epoxy resin harder and more durable. A network structure was formed through radical addition reactions. These cross-linked networks can improve the mechanical properties and chemical stability of epoxy resin (as shown in Figure 11(c<sub>2</sub>)). Shot-peening pretreatment improved the surface roughness and effectively improved the overall adhesion strength of the composite coating (see Figure 11(c<sub>1</sub>)). At the same time, the addition of nanoparticles does not reduce the adhesive strength of the coating nor compensates for the difference in mechanical properties between the substrate and the coating due to its excellent thixotropy, thereby significantly improving the adhesive strength between the nano-composite coating and the substrate. In the knife cutting test, the bond strength was evaluated using the cross-cutting test method (ISO 2409). As shown

in Figure 11(b<sub>2</sub>), according to ASTM standards, there was no peeling phenomenon at the edge of the grid in the coating, and small pieces came off at the intersection of the cuts. The actual damage in the grid area did not exceed 5%, indicating that the adhesive force reached the 4B level and the coating was well bonded to the substrate.

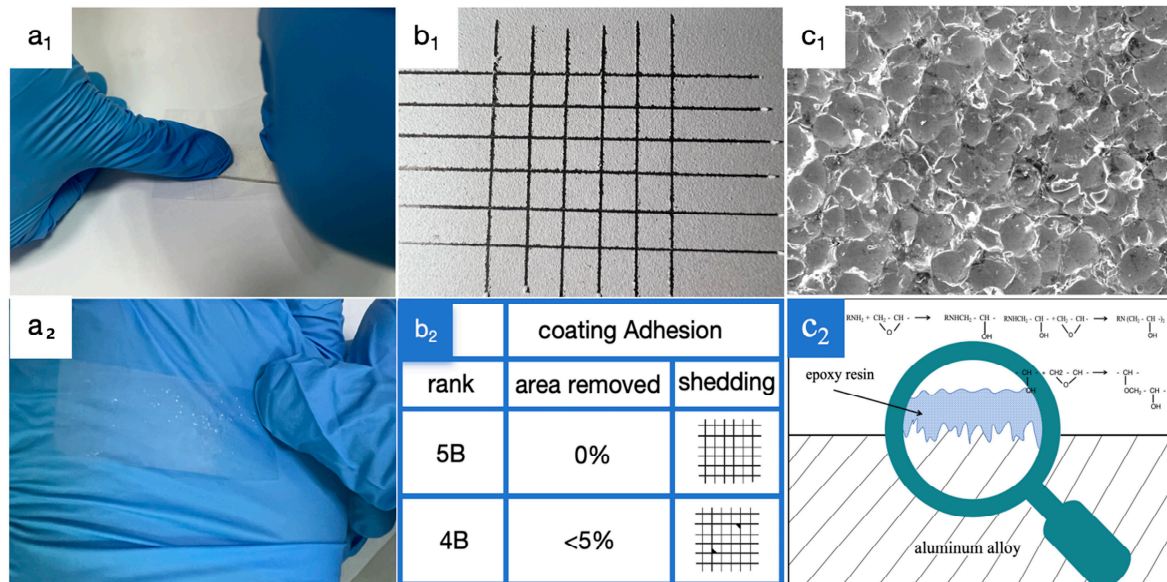


**Figure 11.** (a<sub>1</sub>,a<sub>2</sub>) Tape peeling test. (b<sub>1</sub>,b<sub>2</sub>) Knife scraping test. (c<sub>1</sub>) Shot peening SEM image. (c<sub>2</sub>) Schematic of coating–substrate bonding.

### 3.8. Salt Spray Test for EP-HDTMS@SiO<sub>2</sub> Coatings

The substrate was placed in a closed cabinet at 35 °C (±1) in a salt spray environment created by a 5 wt% NaCl solution to evaluate the corrosion resistance of bare aluminum alloys and coated samples. To complete the test, the corrosion resistance of the bare alloy and EP-HDTMS@SiO<sub>2</sub> coating was tested for 120 h in a neutral salt spray test chamber. The neutral salt spray test showed that the bare aluminum alloy has significantly low corrosion resistance. After 24 h of exposure, a noticeable accumulation of white corrosion oxides can be observed on the surface. Over time, the surface of the alloy became covered with large, loose corrosion products in irregular clumps or foam-like shapes. These corrosion products gradually increased in thickness and expanded outward, ultimately resulting in a significant corrosion area. The XRD analysis showed that the composition of the corrosion product was basically the same, mainly consisting of aluminum alloy and the corrosion product Al<sub>2</sub>O<sub>3</sub>. The composition may include AlO(OH), Al(OH)<sub>3</sub>, and other intermediate phases. As the exposure time increased, the intensity of the Al peak gradually decreased, while the intensity of the Al<sub>2</sub>O<sub>3</sub> peak progressively increased. NaCl showed remarkable hygroscopic properties, with the dissolved Cl<sup>-</sup> ions in a thin liquid film increasing the conductivity of the solution and thus accelerating the corrosion process. At the same time, Cl<sup>-</sup> was an active ion with strong adsorption and erosivity. Cl<sup>-</sup> and O<sub>2</sub> were competitively adsorbed or first adsorbed through a thin liquid film at the active site on the surface of aluminum alloy, then Cl<sup>-</sup> further reacted with Al(OH)<sub>3</sub> to produce water-soluble AlCl<sub>3</sub> (as shown in Figure 12a) [29]. Accordingly, the film layer of the superhydrophobic EP-HDTMS@SiO<sub>2</sub> coating fell off and corrosion products appeared on the substrate surface after 96 h of soaking, indicating that the solution penetrated into the interface of the alloy substrate. At this point, the visible aluminum alloy is still covered by the clear coating, indicating that the coating still provides protection. The experiment was carried out in accordance with the AETM B117-2016 standard and, at that time, the coating had a protection level of 5, which means that there were breaks on the edges. Figure 12d shows the weight change per day for the superhydrophobic EP-HDTMS@SiO<sub>2</sub> coating and the salt spray corrosion of the

substrate. After 24 h of corrosion, 7075 aluminum alloy corrodes heavily and produces more new material due to its low corrosion resistance. The superhydrophobic EP-HDTMS@SiO<sub>2</sub> coating provides excellent protection and the corrosion products slowly increase. Based on all these results, EP-HDTMS@SiO<sub>2</sub> coating significantly improved the corrosion resistance of 7075 aluminum alloy in immersion tests or cyclic wet and dry immersion tests. When the coating is immersed in water, the formation of an air film on the coating surface prevents water droplets from penetrating the microstructure. This air film acts as an additional barrier and effectively isolates the coating from water, soluble ions, and oxygen.

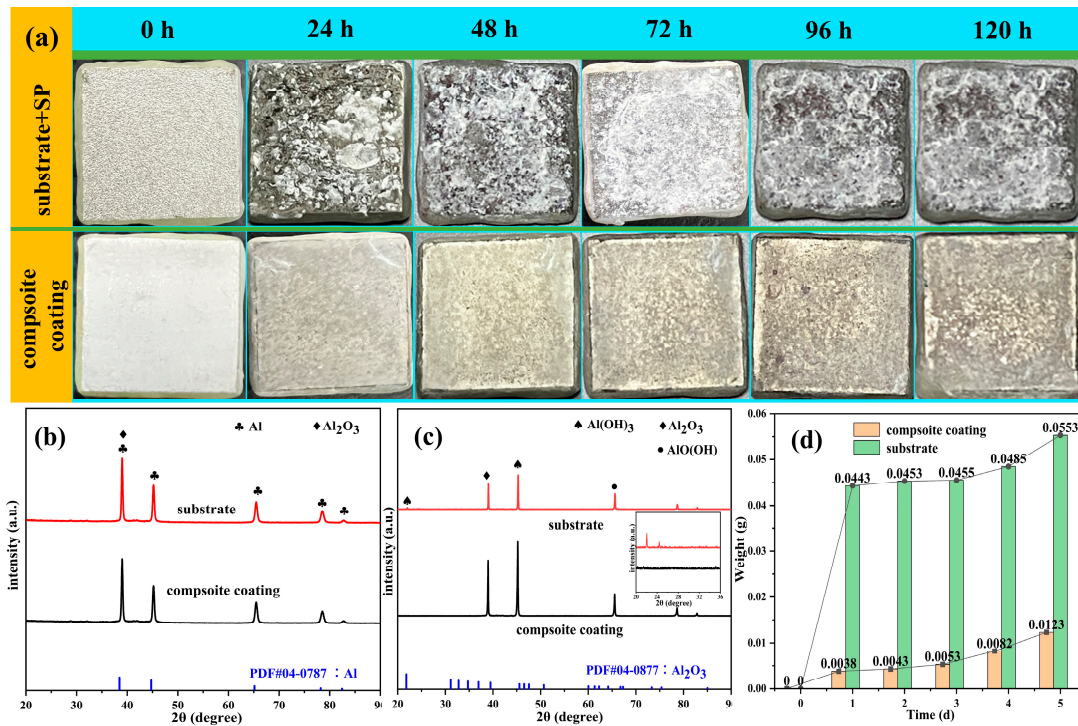


**Figure 12.** (a) Macroscopic morphologies of EP-HDTMS@SiO<sub>2</sub> superhydrophobic coating and substrate in different days under salt spray test. (b,c) EP-HDTMS@SiO<sub>2</sub> XRD before and after salt spray test between superhydrophobic coating and substrate. (d) Weight change of EP-HDTMS@SiO<sub>2</sub> superhydrophobic coating and substrate.

In the salt spray chamber, the salt mist generated consists of ultrafine electrolyte particles that are significantly smaller than the average distance between adjacent micropeak valleys on the coating surface. This creates a high susceptibility for the electrolyte particles to be deposited at the bottom of the cavities between the peaks and valleys, which in turn form the electrolyte layer. The similarity of the size of these electrolyte particles with the microstructure of the coating makes the electrolyte layer between the peaks and valleys more vulnerable to water, which accelerates the aggregation process of the electrolyte particles; this may lead to a reduction in the corrosion resistance of the coating. Furthermore, the corrosion starts from the coating to the substrate and leads to peeling of the edges of the substrate coating.

### 3.9. Mechanism of Ant-Corrosion Resistance for EP-HDTMS@SiO<sub>2</sub> Coatings

The mechanism of EP-HDTMS@SiO<sub>2</sub> coating to improve the ant-corrosion resistance of aluminum alloy against pitting is shown in Figure 13. In the microscopic space, a unique rough surface structure with low surface energy was jointly constructed by mixing epoxy resin, silica, and hexadecyltrimethoxysilane. The EP-HDTMS@SiO<sub>2</sub> coating conformed well to the stable Cassie–Baxter wetting model, and the air present in the rough structure created a stable pore as a physical barrier to prevent corrosion. The nano-scale holes present

on this surface can trap air, block corrosive ions such as  $\text{Cl}^-$ , and prevent direct contact between the substrate and corrosive media. Due to the capillary action in the pores and grooves of the coating, the resulting high capillary negative pressure and antigavity are transmitted more easily; the Laplace pressure, as defined in Formula (1), can push seawater out of the pores, where  $\theta$  is the contact angle,  $\gamma$  is the surface tension,  $g$  is the gravitational acceleration,  $R$  is the capillary radius, and  $\rho$  is the liquid density.

$$H = \frac{2\gamma\cos\theta}{\rho gR} \tag{1}$$

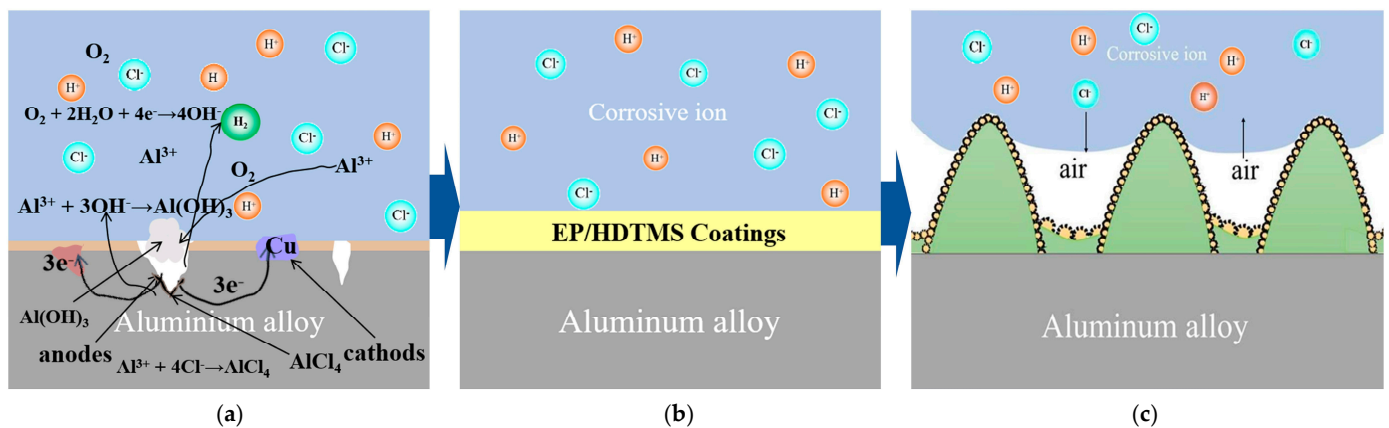


**Figure 13.** (a) Schematic diagram of aluminum alloy pitting corrosion. (b) Schematic diagram of non-added nano-silica coating. (c) EP-HDTMS@SiO<sub>2</sub> coating corrosion resistance schematic diagram.

In addition, during the preparation of the superhydrophobic EP-HDTMS@SiO<sub>2</sub> coating, a large amount of C-H occupies the surface interaction sites, which neatly arranges outward to result in hydrophobicity. Even in long-term corrosive environments, rough surface microstructures can be destroyed and hydrophobic agents can be desorbed, leading to the loss of the first two protection strategies. The organic EP-HDTMS@SiO<sub>2</sub> coating, which mainly consists of epoxy resin, can still effectively suppress the diffusion of corrosive media for a period of time [32].

#### 4. Conclusions

In this study, a superhydrophobic EP-HDTMS@SiO<sub>2</sub> coating was successfully prepared on the surface of shot-peened 7075-T6 alloy. The coating exhibits excellent hydrophobic properties for various liquids, with a maximum static contact angle of 152.6°. In addition, the EP-HDTMS@SiO<sub>2</sub> coating not only has exceptional self-cleaning properties, but also shows good mechanical stability. Electrochemical test results show that the  $E_{\text{CORR}}$  of the superhydrophobic composite coating increased by 0.639 V, while the  $I_{\text{CORR}}$  decreased by four orders of magnitude compared to pure aluminum alloy. In the salt spray corrosion test, the EP-HDTMS@SiO<sub>2</sub> coating maintained its protective performance after 120 h. This research offers a simple method to prepare superhydrophobic coatings with high practical application.

**Author Contributions:** Writing—original draft, R.D., Z.L. and Q.Y.; writing—review and editing, K.Z. and V.J. All authors have read and agreed to the published version of the manuscript.

**Funding:** This research was funded by the National Natural Science Foundation of China grant number 51605293, and the Natural Science Foundation of Shanghai grant number 21ZR14445700, and the Shanghai Sailing Program grant number 21YF1430800.

**Data Availability Statement:** The original contributions presented in the study are included in the article, further inquiries can be directed to the corresponding authors.

**Conflicts of Interest:** The authors declare that they have no known competing financial interests or personal relationships that could have appeared to influence the research reported in this paper.

## References

1. Imran, M.; Khan, A.R.A. Characterization of Al-7075 metal matrix composites: A review. *J. Mater. Res.* **2019**, *8*, 3347–3356. [[CrossRef](#)]
2. Olugbade, T.O.; Omiyale, B.O.; Ojo, O.T.; Adeyeri, M.K. Stress-Corrosion and Corrosion-Fatigue Properties of Surface-Treated Aluminium Alloys for Structural Applications. *Chem. Afr.* **2023**, *6*, 1699–1708. [[CrossRef](#)]
3. Fujii, T.; Ito, D.; Shimamura, Y. Growth characteristics of stress corrosion cracking in high-strength 7075 aluminum alloy in sodium chloride solutions. *Eng. Fract. Mech.* **2023**, *292*, 109657. [[CrossRef](#)]
4. Altenbach, C.; Schnatterer, C.; Mercado, U.A.; Suuronen, J.-P.; Zander, D.; Requena, G. Synchrotron-based holotomography and X-Ray fluorescence study on the stress corrosion cracking behavior of the peak-aged 7075 aluminum alloy. *J. Alloys Compd.* **2020**, *817*, 152722. [[CrossRef](#)]
5. Yang, M.; Lei, L.; Jiang, Y.; Xu, F.; Yin, C. Simultaneously improving tensile properties and stress corrosion cracking resistance of 7075-T6 aluminum alloy by USRP treatment. *Corros. Sci.* **2023**, *218*, 111211. [[CrossRef](#)]
6. Wang, C.; Wang, C.; Wang, L.; Lai, Y.; Li, K.; Zhou, Y. A dislocation density-based comparative study of grain refinement, residual stresses, and surface roughness induced by shot peening and surface mechanical attrition treatment. *Int. J. Adv. Manuf. Technol.* **2020**, *108*, 505–525. [[CrossRef](#)]
7. Sun, S.; Fang, Y.; Zhang, L.; Li, C.; Hu, S. Effects of aging treatment and peripheral coarse grain on the exfoliation corrosion behaviour of 2024 aluminium alloy using SR-CT. *J. Mater. Res.* **2020**, *9*, 3219–3229. [[CrossRef](#)]
8. Bao, L.; Li, K.; Zheng, J.; Zhang, Y.; Zhan, K.; Yang, Z.; Zhao, B.; Ji, V. Surface characteristics and stress corrosion behavior of AA 7075-T6 aluminum alloys after different shot peening processes. *Surf. Coat. Technol.* **2022**, *440*, 128481. [[CrossRef](#)]
9. Tian, W.; Chao, B.; Xiong, X.; Li, Z. Effect of Surface Roughness on Pitting Corrosion of 2A12 Aluminum Alloy. *Int. J. Electrochem. Sci.* **2018**, *13*, 3107–3123. [[CrossRef](#)]
10. Chi, G.; Yi, D.; Liu, H. Effect of roughness on electrochemical and pitting corrosion of Ti-6Al-4V alloy in 12 wt.% HCl solution at 35 °C. *J. Mater. Res. Technol.* **2020**, *9*, 1162–1174. [[CrossRef](#)]
11. Oh, S.; Kim, D.; Kim, K.; Kim, D.-I.; Chung, W.; Shin, B.-H. The effect of surface roughness on re-passivation and pitting corrosion of super duplex stainless steel UNS S 32760. *Int. J. Electrochem. Sci.* **2023**, *18*, 100351. [[CrossRef](#)]
12. Sajid, H.U.; Kiran, R. Influence of corrosion and surface roughness on wettability of ASTM A36 steels. *J. Constr. Steel Res.* **2018**, *144*, 310–326. [[CrossRef](#)]
13. Walter, R.; Kannan, M.B. Influence of surface roughness on the corrosion behaviour of magnesium alloy. *Mater. Des.* **2011**, *32*, 2350–2354. [[CrossRef](#)]
14. Vazirinasab, E.; Jafari, R.; Momen, G. Application of superhydrophobic coatings as a corrosion barrier: A review. *Surf. Coat. Technol.* **2018**, *341*, 40–56. [[CrossRef](#)]
15. Latthe, S.S.; Sutar, R.S.; Kodag, V.S.; Bhosale, A.K.; Kumar, A.M.; Kumar Sadasivuni, K.; Xing, R.; Liu, S. Self-cleaning superhydrophobic coatings: Potential industrial applications. *Prog. Org. Coat.* **2019**, *128*, 52–58. [[CrossRef](#)]
16. Lee, D.; Lim, J.W.; Lee, D.G. Cathode/anode integrated composite bipolar plate for high-temperature PEMFC. *Compos. Struct.* **2017**, *167*, 144–151. [[CrossRef](#)]
17. Huang, W.; Huang, J.; Guo, Z.; Liu, W. Icephobic/anti-icing properties of superhydrophobic surfaces. *Adv. Colloid. Interface Sci.* **2022**, *304*, 102658. [[CrossRef](#)]
18. Luo, G.; Wen, L.; Yang, K.; Li, X.; Xu, S.; Pi, P.; Wen, X. Robust and durable fluorinated 8-MAPOSS-based superamphiphobic fabrics with buoyancy boost and drag reduction. *Chem. Eng. J.* **2020**, *383*, 123125. [[CrossRef](#)]
19. Yang, Q.; Cao, J.; Ding, R.; Zhan, K.; Yang, Z.; Zhao, B.; Wang, Z.; Ji, V. The synthesis and mechanism of superhydrophobic coatings with multifunctional properties on aluminum alloys surface: A review. *Prog. Org. Coat.* **2023**, *183*, 107786. [[CrossRef](#)]
20. Rasitha, T.P.; Krishna, D.N.G.; Thinaharan, C.; Vanithakumari, S.C.; Philip, J. Optimization of coating parameters for fabrication of robust superhydrophobic (SHP) aluminum and evaluation of corrosion performance in aggressive medium. *Prog. Org. Coat.* **2022**, *172*, 107076. [[CrossRef](#)]
21. Abu Jarad, N.; Imran, H.; Imani, S.M.; Didar, T.F.; Soleymani, L. Fabrication of Superamphiphobic Surfaces via Spray Coating; a Review. *Adv. Mater. Technol.* **2022**, *7*, 2101702. [[CrossRef](#)]
22. Zou, D.; Xiao, L.; Zhang, Y.; Li, H. Effect of hexadecyltrimethoxysilane modified micro silica particles on workability and compressive strength of ultra-high-performance concrete. *Constr. Build. Mater.* **2023**, *399*, 132480. [[CrossRef](#)]
23. Ren, T.; Tang, G.; Yuan, B.; Yang, Y.; Yan, Z.; Ma, L.; Huang, X. Hexadecyltrimethoxysilane-Modified SiO<sub>2</sub> Nanoparticle-Coated Halloysite Nanotubes Embedded in Silicone-Acrylic Polymer Films as Durable Fluorine-Free Superhydrophobic Coatings. *ACS Appl. Nano Mater.* **2020**, *3*, 5807–5815. [[CrossRef](#)]
24. Jeong, E.; Woo, H.; Moon, Y.; Lee, D.Y.; Jung, M.; Lee, Y.-S.; Bae, J.-S. Self-Cleaning Polyester Fabric Prepared with TiO<sub>2</sub> and Hexadecyltrimethoxysilane. *Polymers* **2021**, *13*, 387. [[CrossRef](#)]
25. Dai, X.; Yang, F.; Yang, R.; Huang, X.; Rigdon, W.A.; Li, X.; Li, C. Biphilic nanoporous surfaces enabled exceptional drag reduction and capillary evaporation enhancement. *Appl. Phys. Lett.* **2014**, *105*, 191611. [[CrossRef](#)]

26. Dai, X.; Huang, X.; Yang, F.; Li, X.; Sightler, J.; Yang, Y.; Li, C. Enhanced nucleate boiling on horizontal hydrophobic-hydrophilic carbon nanotube coatings. *Appl. Phys. Lett.* **2013**, *102*, 161605. [[CrossRef](#)]
27. Li, X. Nanoscale structural and mechanical characterization of natural nanocomposites: Seashells. *JOM* **2007**, *59*, 71–74. [[CrossRef](#)]
28. Li, F.; Nan, S.; Zhu, R.; Yao, R.; Wang, H.; Zhang, T.; Zhang, J. Abundant octadecylamine modified epoxy resin for superhydrophobic and durable composite coating. *Sustain. Mater. Technol.* **2023**, *37*, e00690. [[CrossRef](#)]
29. Wang, Y.; Ou, B.; Zhu, P.; Niu, B.; Guo, Y.; Zhi, Q. High mechanical strength aluminum foam epoxy resin composite material with superhydrophobic, anticorrosive and wear-resistant surface. *Surf. Interfaces* **2022**, *29*, 101747. [[CrossRef](#)]
30. Zhao, Q.; Zhao, X.; Jin, Z.; Wang, P.; Fan, L.; Deng, J.; Yuan, S.; Sun, Y.; Duan, J. Mechanism of an organic-inorganic composite coating with anticorrosive and versatile superhydrophobic properties: A combined electrochemical and molecular dynamics exploration. *Prog. Org. Coat.* **2023**, *182*, 107610. [[CrossRef](#)]
31. Liu, P.; Yang, F.; Zhang, R.; Zhou, H.; Wang, Y.; Cheng, Y. Fabrication of superhydrophobic coating on brass based on polysiloxane and expanded vermiculite via spraying method and its excellent environmental adaptability. *Prog. Org. Coat.* **2023**, *182*, 107670. [[CrossRef](#)]
32. Le Guen-Geffroy, A.; Le Gac, P.Y.; Habert, B.; Davies, P. Physical ageing of epoxy in a wet environment: Coupling between plasticization and physical ageing. *Polym. Degrad. Stab.* **2019**, *168*, 108947. [[CrossRef](#)]

**Disclaimer/Publisher's Note:** The statements, opinions and data contained in all publications are solely those of the individual author(s) and contributor(s) and not of MDPI and/or the editor(s). MDPI and/or the editor(s) disclaim responsibility for any injury to people or property resulting from any ideas, methods, instructions or products referred to in the content.